32. Nabha SM, dos Santos EB, Yamamoto HA, Belizi A, Dong Z, Meng H, et al. Bone marrow stromal cells enhance prostate cancer cell invasion through type I collagen in an MMP-12-dependent manner. Int J Cancer 2008;122:2482-2490.

33. Miyata Y, Iwata T, Maruta S, Kanda S, Nishikido M, Kaga S, et al. Expression of matrix metalloproteinase-10 in renal cell carcinoma and its prognostic role. Eur Urol 2007;52:791-797.

34. Kessenbrock K, Plaks V, Werb Z. Matrix metalloproteinases: regulators of the tumor microenvironment. Cell 2010;141:52-67.

35. Romualdez AG Jr, Ward PA. A unique complement derived chemotactic factor for tumor cells. Proc Nat Acad Sci USA 1975;72:4128-4132.

36. Orr W, Phan SH, Varani J, Ward PA, Kreutzer DL, Webster RO, et al. Chemotactic factor for tumor cells derived from the C5a fragment of complement component C5. Proc Natl Acad Sci USA 1979;76:1986-1989.

37. Schiefeldecker HL, Schlaf G, Koleva M, Götze O, Jungermann K. Induction of functional anaphylatoxin C5a receptors on hepatocytes by in vivo treatment of rats with IL-6. J Immunol 2000;164:5453-5458.

38. Takeyama H, Wakamiya N, O'Hara C, Arthur K, Niloff J, Kufe D, et al. Tumor necrosis factor expression by human ovarian carcinoma in vivo. Cancer Res 1991;51:4476-4480.

39. Maeda H, Fang J, Inutsuka T, Kitamoto Y. Vascular permeability enhancement in solid tumors: various factors, mechanisms involved and its implications. Int Immunopharmacol 2003;3:319-328.

40. Hall A. Rho GTPases and the actin cytoskeleton. Science 1998;279:509-514.

41. Nobes CD, Hall A. Rho, Rac, and Cdc42 GTPases regulate the assembly of multimolecular focal complexes associated with actin stress fibers, lamellipodia, and filopodia. Cell 1995;81:53-62.

42. Li Z, Hannigan M, Mo Z, Liu B, Lu W, Wu Y, et al. Directional sensing requires Gβγ-mediated PAK1 and PIXα-dependent activation of Cdc42. Cell 2003;114:215-227.

Figure legends

Figure 1. Expression of C5aR in human primary cancers. ***A***, Human cancer tissues were immunohistochemically stained with an anti-C5aR antibody or control IgG (inset), and representative examples are shown. Colon cancer (top left) and normal colon epithelium (top right); esophagus normal epithelium (bottom, encircled) and cancer (bottom, not encircled). Scale bars = 50 μm. ***B***, Cancer cell C5aR-positive case ratios (positive cases/total cases examined) (•) in primary organs. The vertical scale bar shows the 95% confidence interval that is estimated from the binominal proportion based on the beta distribution. EP, esophagus (n = 20); ST, stomach (n = 20); Col, colon (n = 40); Liv, liver (n = 20); BD, bile ducts (n = 46); Pan, pancreas (n = 10); Kid, kidney (n = 11); UB, urinary bladder (n = 45); Lun, lung (n = 12); PT, prostate (n = 25); Mam, mammary gland (n = 21).

Figure 2. Expression of C5aR on cancer cell lines including HuCCT1/C5aR and HuCCT1/mock. ***A***, Expression of C5aR mRNA in several cancer cell lines shown by RT-PCR. ***B***, Expression of C5aR protein in bile duct and colon cancer cell lines, shown

by immunoblotting using an anti-C5aR antibody. β-actin mRNA and protein were used as controls. ***C***, Expression of C5aR on the cell membrane in MEC and HuCCT1/C5aR, shown by flow cytometry using FITC-conjugated anti-C5aR antibody (gray line) or control antibody (black line).

Figure 3. C5a elicits C5aR expressing cancer cells by inducing cytoskeletal reorganization and changes in cellular morphology. ***A***, HuCCT1/C5aR and HuCCT1/mock cells were incubated with C5a (100 nM) and fixed at indicated time points. F-actin was visualized by immunofluorescence staining with Alexa 488-conjugated Phalloidin. Scale bars: 20 μm. Arrow head and an arrow indicate filopodia and membrane ruffling, respectively. ***B***, Time Lapse analysis of cell motility. Cell images taken at 0, 3, 6 and 9 h are shown. Broken circles indicate the initial cell position shown at 0 h. ***C***, Cell migration distance was measured by tracing a cell. $^{*}P < 0.01$ ($n = 6$).

Figure 4. Enhancement of C5aR-expressing cancer cell invasion by C5a *in vitro*.

Cancer cell invasion was measured by the Matrigel invasion chamber assay. HuCCT1-derived (***A***) or MEC cells (***B***) were placed in the upper chamber and medium supplemented with various concentrations of C5a was placed in the lower chamber. HuCCT1-derived (***C***) or MEC cells (***D***) were pretreated with various concentrations of C5a for 12 h and 24 h respectively. These cells were washed and were placed in the upper chamber, and medium was placed in the lower chamber. Incubation time for assay: 24 h (***A***, ***C***) and 36 h (***B***, ***D***). (□), HuCCT1/mock (***A***, ***C***); (■), HuCCT1/C5aR (***A***, ***C***); crosshatched and closed bars (***B***, ***D***) indicate MEC cells treated with anti-C5aR antibody or nonspecific IgG, respectively. Gray bars (***A***, ***B***) indicates cells incubated in the upper chamber in the presence of GM6001 (5 μM). ***E***. Checkerboard analysis for C5a cancer cell invasion activity. Closed, crosshatched and open bars indicate C5a concentration 0, 10 or 100 nM, respectively, in the lower chamber.*, $p < 0.01$; n.s., not significant.

Figure 5. Enhanced invasiveness of C5aR-expressing cancer cells by C5a *in vivo*. HuCCT1/C5aR and HuCCT1/mock cells were incubated separately in the presence or

absence of 100 nM C5a (C5a(+) or C5a(-), respectively) for 12 h. After washing, cells were labeled, mixed, and injected together into nude mouse skin. ***A***. Distribution of HuCCT1/C5aR (*orange*) and HuCCT1/mock (*green*) cells in nude mouse skin two days after implantation. Right panels are corresponding sections stained with hematoxylin-eosin. Bars = 300 μm. ***B***. Cell distribution square ratio (HuCCT1/C5aR cells versus HuCCT1/mock cells). Cells were incubated in the presence (■) or absence (□) of C5a. *, $p < 0.01$ ($n = 5$).

Figure 1

A

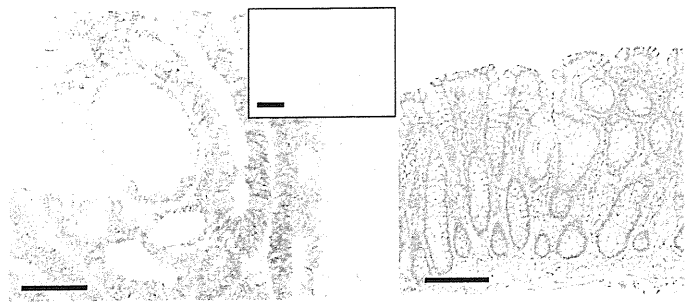

colon

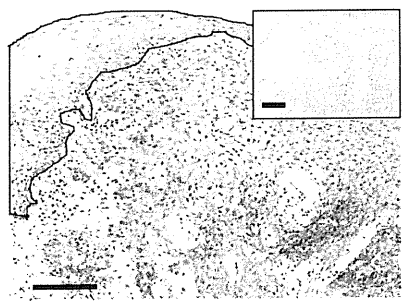

esophagus

B

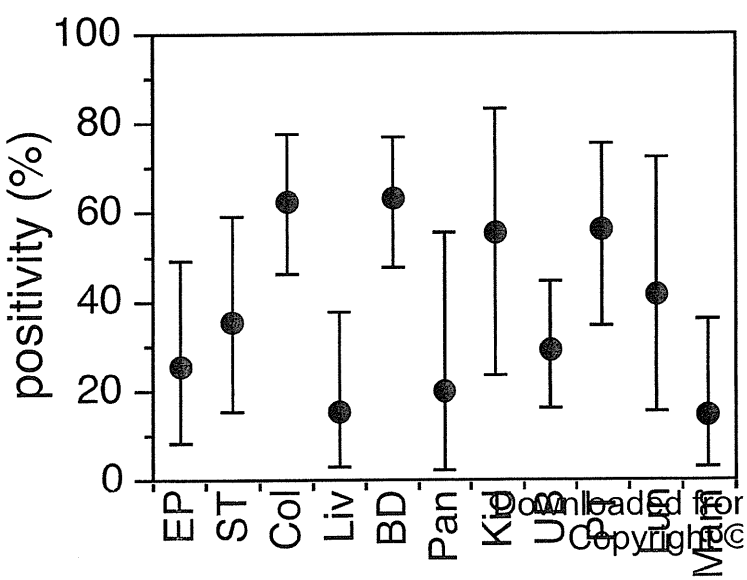

Figure 2

A

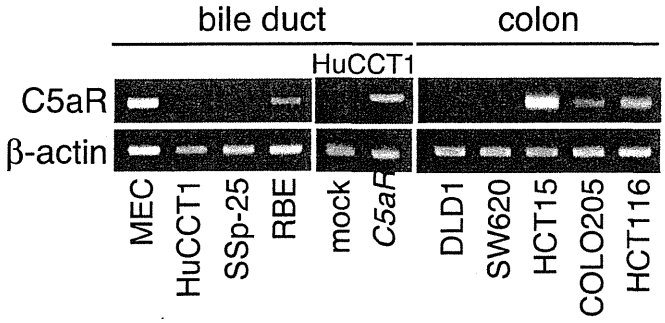

B

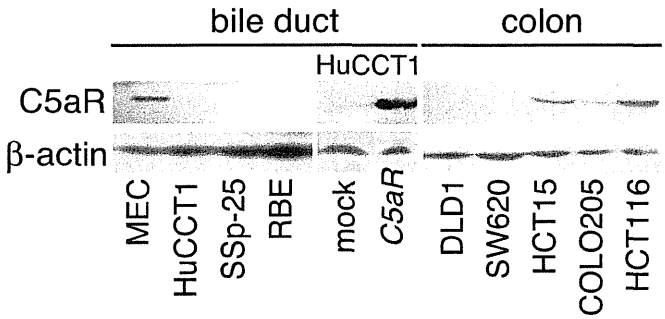

C

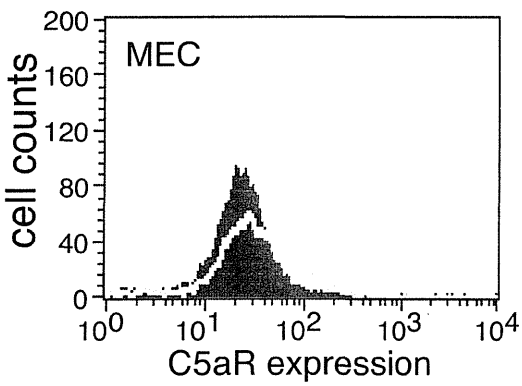

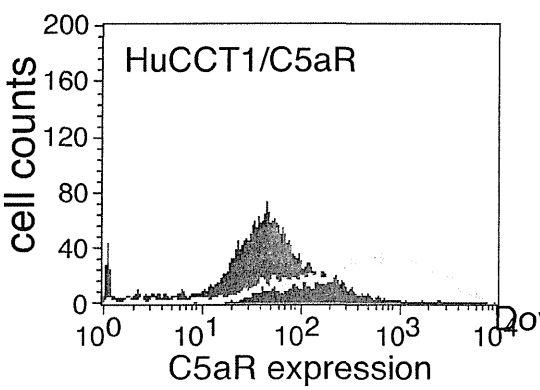

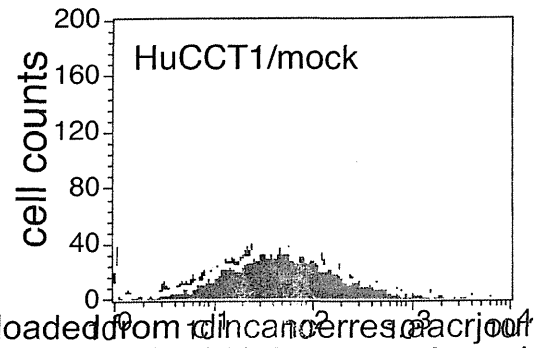

Figure 3

A

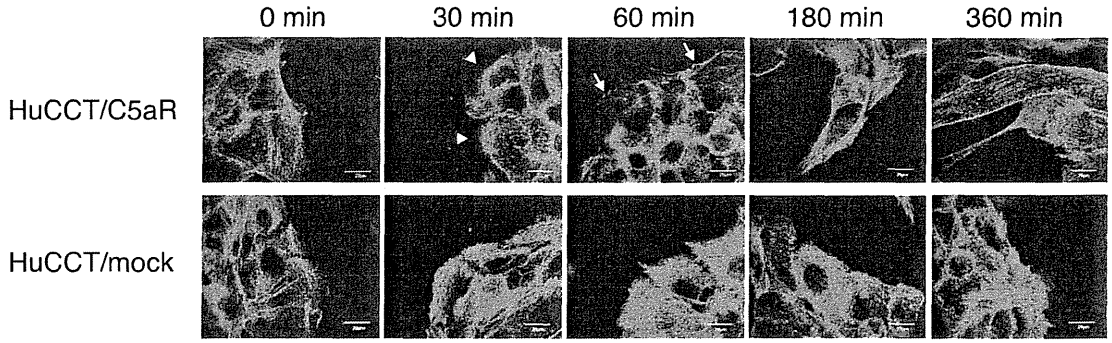

B

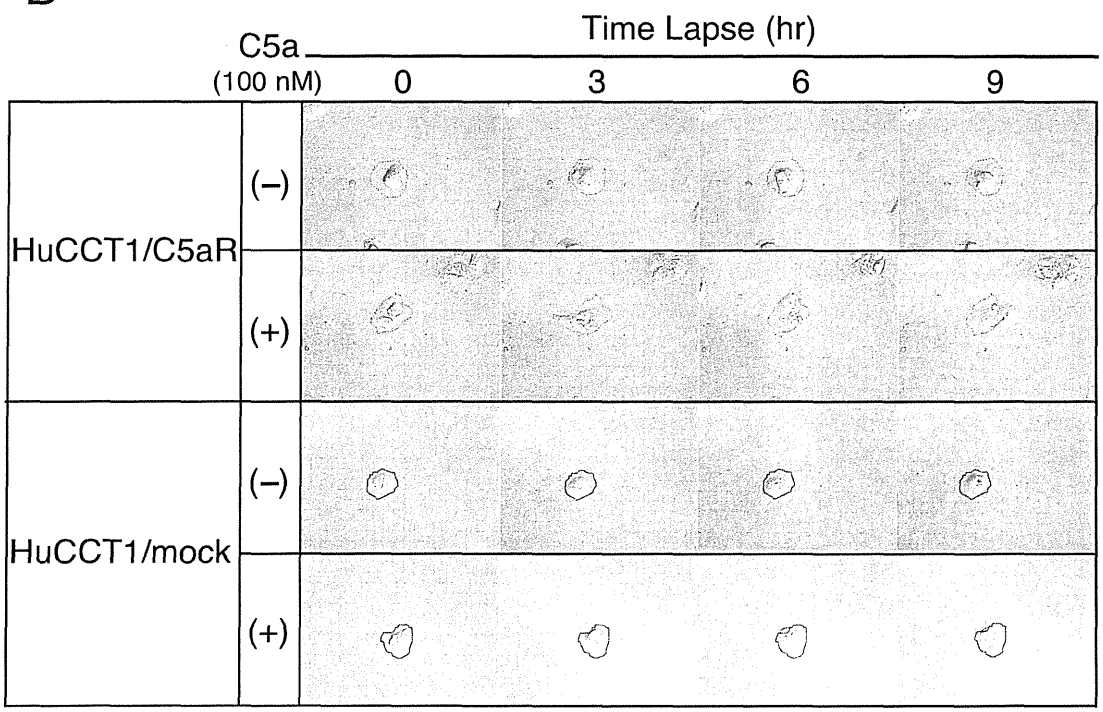

C

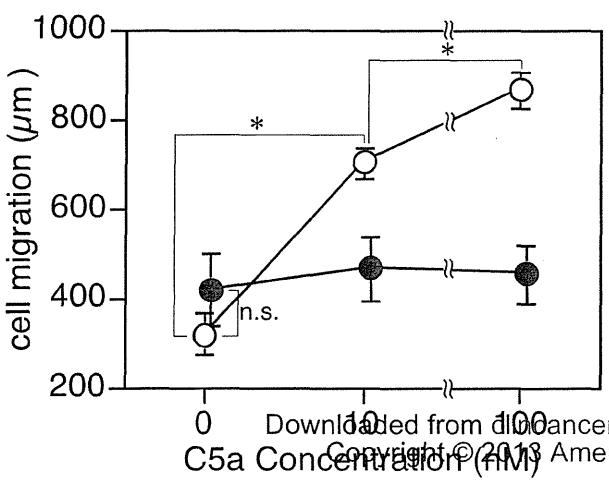

Figure 4

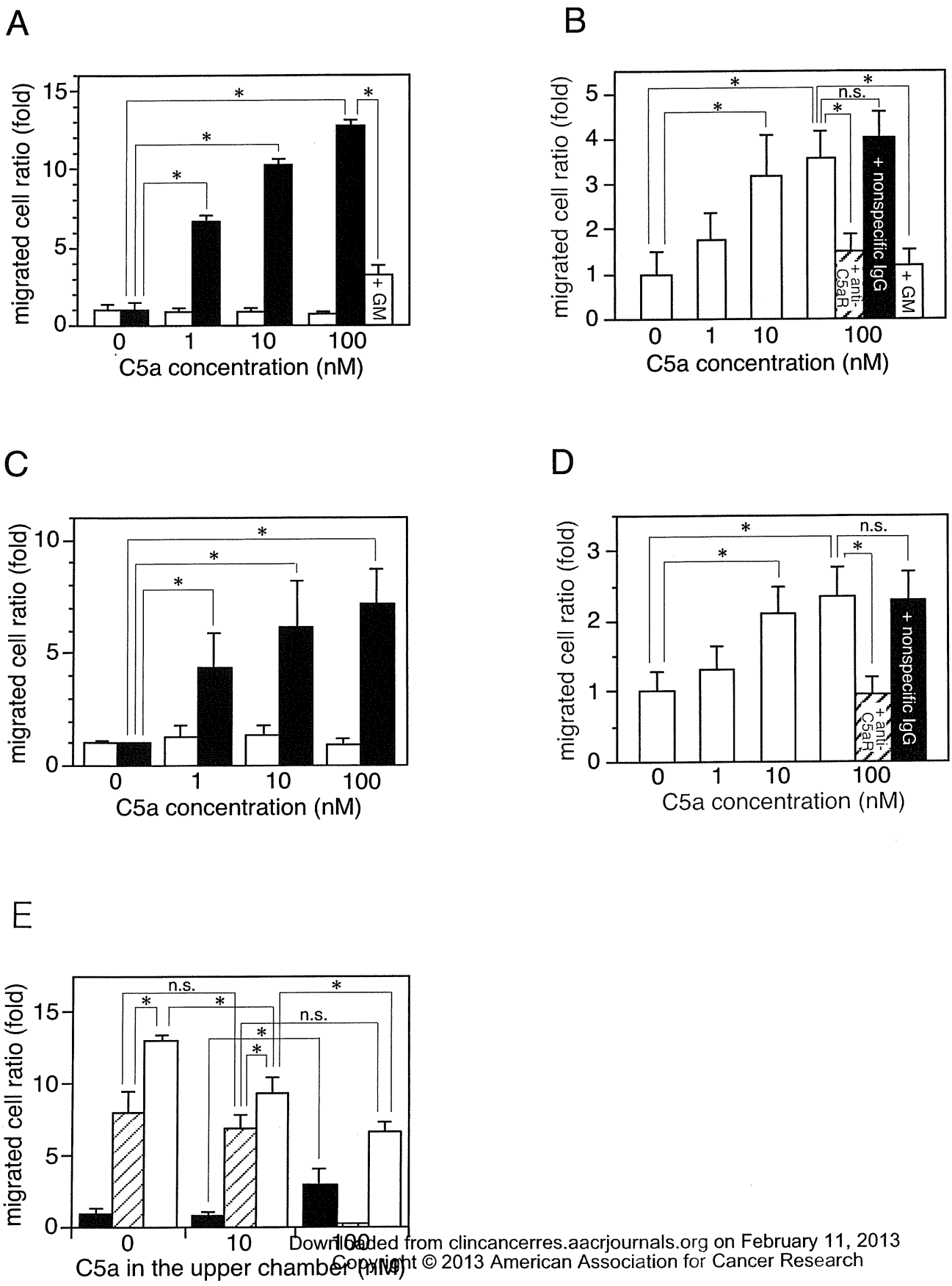

Figure 5

A

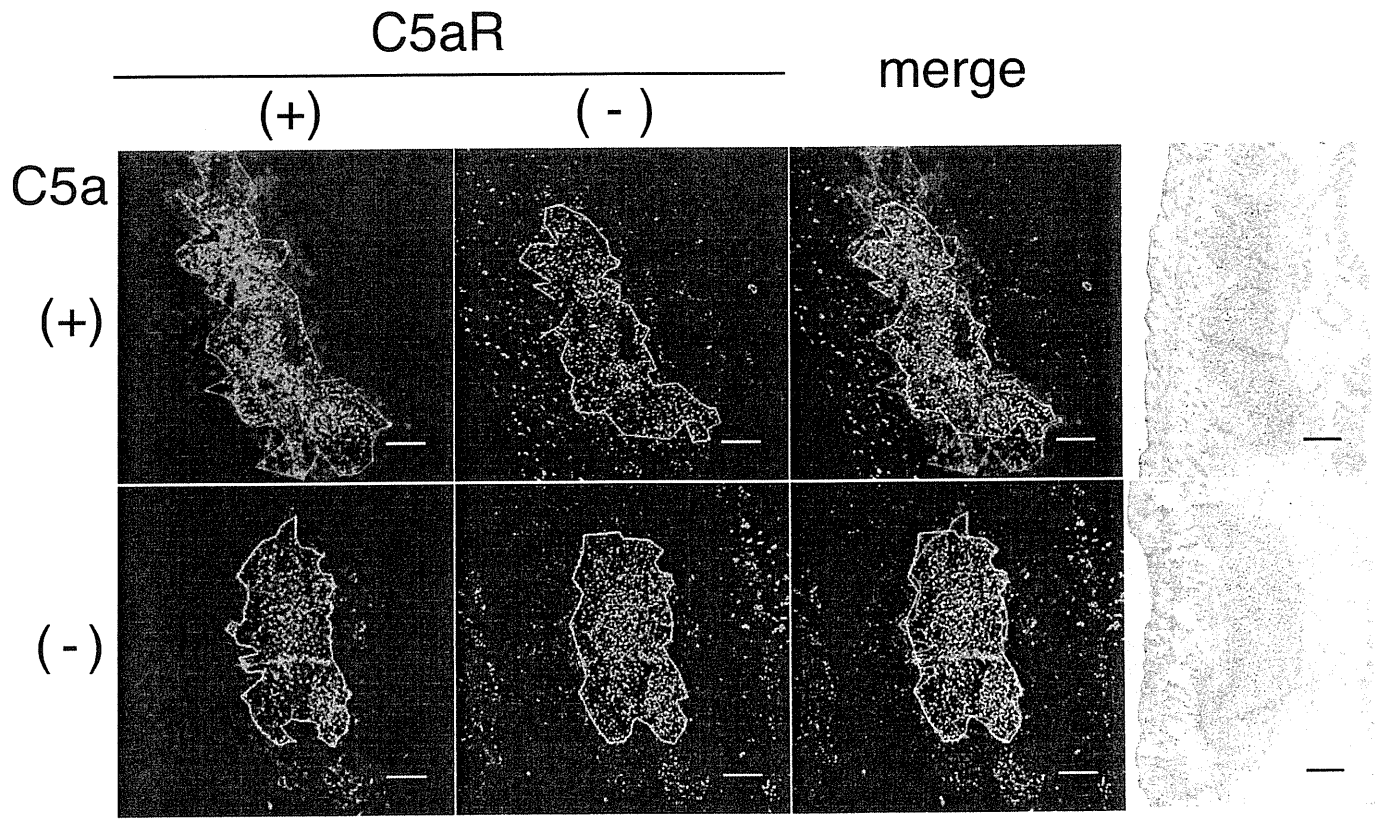

B

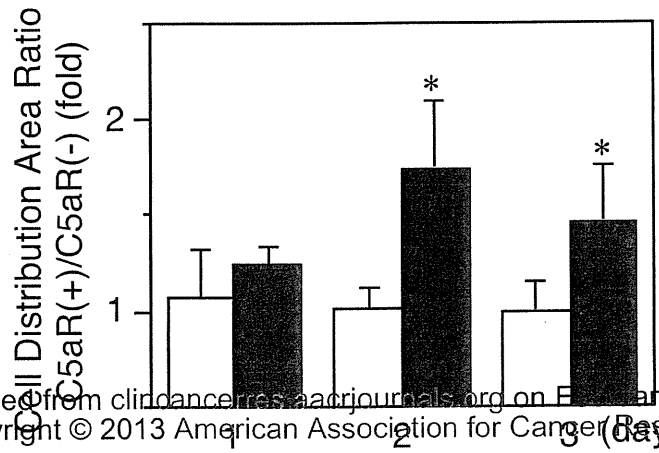

Author Manuscript Published OnlineFirst on January 3, 2013; DOI:10.1158/1078-0432.CCR-12-1204
Author manuscripts have been peer reviewed and accepted for publication but have not yet been edited.

Table 1. C5a-stimulated MMP release from C5aR expressing cancer cells.

	MEC			HuCCT1/C5aR		
MMP	C5a (-)[a]	C5a (+)[a]	Ratio[b]	C5a (-)[a]	C5a (+)[a]	Ratio[b]
1	149332.6±17039	291140.4±5360.4*	1.95	88906.6±27436.8	129408±3485	1.46
2	32.5±11.3	116.9±67. 8	3.59	1220.4±184.3	870.7±73	0.71
3	26.8±12.0	134.7±42.1*	5.03	971.6±224.6	927.5±162.9	0.95
8	20.1±23.6	74.9±29.9	3.72	335.6±77.7	1128.3±120.9*	3.36
9	< 0.1[c]	12.3±3.6*	-	6105.1±2011.3	6213.4±4357.7	1.02
10	857.6±740.5	9301.4±641.8*	10.84	57641.4±5197.5	111666.4±7911.1*	1.94
13	359.2±118.7	1367.3±309.3*	3.80	1411.9±154.6	1642.8±287	1.16

[a] MMP concentrations (pg/mL) in culture supernatants of cancer cells cultured for 24 h in the presence (+) or absence (-) of C5a (100 nM). [b] ratio of C5a(+) versus C5a(-) in mean values. [c] below the detection limit. *$P < 0.01$ ($n = 4$).

JJCO Japanese Journal of Clinical Oncology

Jpn J Clin Oncol 2012;42(12)1232

Image of the Month

A Case of Peritoneal Dissemination of High-grade Small Round Cell Sarcoma

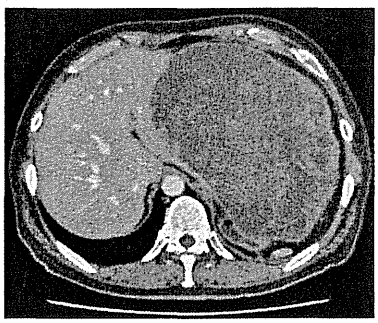

Figure 1.

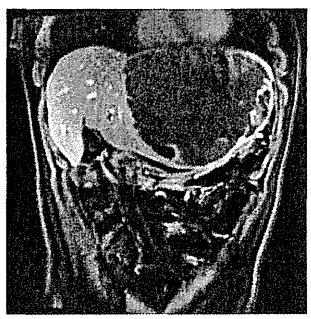

Figure 2.

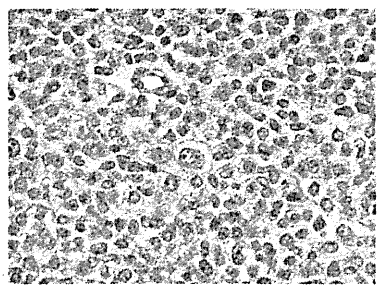

Figure 3.

A 46-year-old man, who had undergone resection of intra-abdominal tumor combined with part of the small bowel and ascending colon at another hospital 1 month before, was referred to our institution. After pathological examination of the resected specimen, the tumor was suspected to be high-grade small round cell sarcoma, presumably arising from the ileocecal mesentery. After referral to our hospital, six cycles of chemotherapy, composed of doxorubicin and ifosfamide, were administered, because imaging studies showed multiple residual intra-abdominal disseminations of the tumor. After chemotherapy, the size and number of the disseminative tumors had decreased. However, 6 months later, the patient complained of exaggerating left upper abdominal pain. Computed tomography (CT) and magnetic resonance imaging (MRI) demonstrated a rapidly enlarging mass of ~20 cm in diameter in the left subphrenic space (Fig. 1: axial CT image; Fig. 2: coronal MRI image). Intra-tumoral hemorrhage was suspected because laboratory tests showed progressive severe anemia (hemoglobin level declined to 5.9 g/dl). Although several other intra-abdominal tumors were recognized, excision of the largest subphrenic tumor was conducted in order to prevent tumor rupture and life-threatening bleeding. Total gastrectomy, left lateral bisegmentectomy (segments 2 and 3) of the liver and partial resection of the diaphragm were necessary for complete resection of the tumor.

Pathologically, the tumor consisted of small round cells with negative immunohistochemical reactivity for AE1/3, EMA and desmin. Finally, the diagnosis of high-grade small round cell sarcoma was made (Fig. 3).

The postoperative course was uneventful, but the patient died ~1 month after the surgery due to multiple liver metastases and rapid growth of residual tumors.

Tsugumasa Kamata and Satoshi Nara
Hepatobiliary and Pancreatic Surgery Division
National Cancer Center Hospital
Tokyo, Japan
doi:10.1093/jjco/hys198